

RESEARCH ARTICLE

Mode-adaptive control of a kilowatt-level large-mode-area fiber laser based on 5×1 photonic lantern

Wenguang Liu^{1,2,3,†}, Yanyang Hu^{1,2,3,†}, Hanwei Zhang^{1,2,3}, Lianchuang Ding^{1,2,3}, Pengfei Liu^{1,2,3}, Baozhu Yan^{1,2,3}, Jiangbin Zhang^{1,2,3}, Qiong Zhou^{1,2,3}, and Zongfu Jiang^{1,2,3}

¹College of Advanced Interdisciplinary Studies, National University of Defense Technology, Changsha, China

²Nanhu Laser Laboratory, National University of Defense Technology, Changsha, China

³Hunan Provincial Key Laboratory of High Energy Laser Technology, Changsha, China

(Received 30 March 2025; revised 9 June 2025; accepted 22 July 2025)

Abstract

This study presents high-power mode-selective operation in a large-mode-area (LMA) fiber laser. A spatial mode-adaptive control system incorporating a 5×1 photonic lantern was employed to facilitate mode conversion between the LP₀₁ and LP₁₁ modes. The coherence length between the five single-mode arms and the stimulated Brillouin scattering threshold in the amplifier were well balanced by tuning the seed linewidth. In addition, the specific design of the fiber amplifier's bending radius enabled stable mode-selective output with high mode purity. Consequently, a near-fundamental mode control was achieved in a 42- μm LMA fiber laser, yielding a beam quality M^2 factor of 1.97 at an output power of 1 kW. Subsequently, a stable LP₁₁ mode laser output with an output power of 219 W and an optical conversion efficiency of 75% was obtained. This research provides a significant technical foundation for the mode-selective operation of high-power LMA fiber lasers.

Keywords: adaptive optics; fiber amplifier; large-mode-area fiber; photonic lantern

1. Introduction

Fiber lasers have garnered significant attention for their wide application in industrial manufacturing, defense, and scientific research^[1–6]. However, scaling up the power of fiber lasers while maintaining near-diffraction-limited beam quality remains a major challenge due to nonlinear effects, such as stimulated Brillouin scattering (SBS) and stimulated Raman scattering (SRS)^[7–9]. Large-mode-area (LMA) fiber lasers offer a potential solution by enhancing the SBS and SRS thresholds through reduced laser intensity in the core. Nevertheless, a larger core size introduces dynamic mode coupling between the fundamental mode (FM) and higher-order modes (HOMs). The increase in modal contents degrades the beam quality^[10–13], posing a significant challenge for LMA fiber lasers to maintain FM operation^[14–16].

The photonic lantern (PL) has emerged as a promising solution for mode control in LMA fiber lasers, providing a new technical approach to achieve high output power with an FM^[17–21]. In 2017, Lincoln Laboratory demonstrated adaptive mode control using a 3×1 PL, achieving a pump-limited 1.27 kW output power in a 25/400 μm gain fiber amplifier^[22]. This technology holds potential for further mode control of high-power fiber lasers with larger core size. However, the team at MIT concluded that the number of input ports of PLs must be equal to the number of modes in the fiber amplifier. Therefore, based on this inference, we can anticipate that when employing a PL to achieve mode control in a LMA fiber with a 42- μm core diameter, where the number of modes will increase to 20 (with a numerical aperture (NA) of 0.069), the input ports of the PL will significantly increase, rendering the control system highly complex and costly^[23]. Therefore, how to achieve effective mode control in LMA fibers using the minimum number of control ports has become a significant technical challenge for practical application. Subsequent research by our group has found that the mode control of LMA fibers can be realized with fewer control ports. In 2024, Ze *et al.*^[24] experimentally

Correspondence to: H. Zhang and Y. Hu, College of Advanced Interdisciplinary Studies, National University of Defense Technology, Changsha 410073, China. Emails: zhanghanwei100@163.com (H. Zhang); ceastbons@163.com (Y. Hu)

[†]These authors contributed equally to this work.

demonstrated mode control in a 42/400 μm fiber laser with a 3×1 PL. However, the SBS and thermal lenses limit the power scaling. Meanwhile, as the core size increases, there is a significant rise in the number of HOMs; the M^2 factor of 2.2 was achieved in Ze *et al.*'s work. This shows that there are considerable challenges to realize high power and near FM output with fewer control ports of PLs.

In this work, we achieved enhanced control results over the HOMs of LMA at kilowatt-level output power with the combination of active and passive control methods. The 5×1 PL possesses greater control capability for HOMs, and bending of the fiber amplifier enables effective filtering out of HOMs in 42- μm gain fibers. The coherence length and SBS threshold were well balanced by optimizing the linewidth of the seed source. In the experiment, the M^2 factor of 1.97 at an output power of 1 kW is achieved. Further power scaling was pump-limited at the 1-kW level. We also achieved the control of LP_{11} with an output power of 219 W, and verified the possibility of HOM operation by mode control technology. This study provides a technical basis for further research on mode-adaptive control of higher-power fiber lasers with fewer-port PLs.

2. Principle of mode control with the PL

The PL is an all-fiber passive optical device that connects a bundle of single-mode fibers (SMFs) and a multi-mode fiber (MMF)^[25]. The structure of the 5×1 PL is shown in Figure 1. As the number of PL input ports increases, the complexity of fabrication correspondingly escalates. In order to optimize the mode evolution process of the PL, it is necessary to strictly control two structural parameters. The first is the lateral dimension, in which the cladding of SMFs is required to corrode from 10/125 to 10/90 μm , and the inner diameter of the low-index capillary tube is reduced to 30 μm with the double tapering process. The second is the longitudinal dimension, in which the long taper region (20 mm) of the 5×1 PL facilitates highly efficient mode evolution.

The unique structure of PLs enables a mode-selective operation. The PL can be effectively approximated as an optical linear converter that facilitates the transition between the FM and HOMs. This conversion process can be mathematically

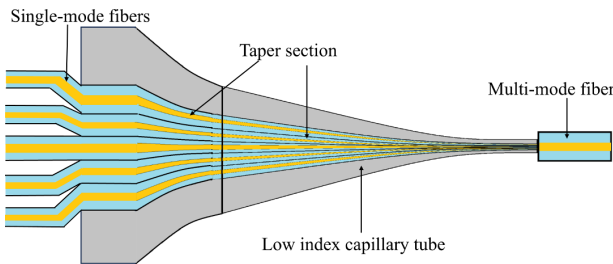


Figure 1. Structure of the 5×1 photonic lantern using the double tapering method.

represented using a transmission matrix. The relationship between the input and output ports of the PL is expressed as follows: $Av = u$, where $v^T = [v_1 e^{j\theta_1}, v_2 e^{j\theta_2}, \dots, v_i e^{j\theta_i}]$ is the column vector describing the optical field of the SMFs (v_i, θ_i represent the amplitude and phase of the i th input ports, respectively), $u^T = [u_1 e^{j\theta_1}, u_2 e^{j\theta_2}, \dots, u_n e^{j\theta_n}]$ is the column vector describing the optical field of the MMF (u_n, θ_n represent the amplitude and phase of the LP_{nm} mode, respectively) and A is the transmission matrix of the PL:

$$A = \begin{bmatrix} 0.4e^{i(0\pi)} & 0.4e^{i(0\pi)} & 0.4e^{i(0\pi)} & 0.4e^{i(0\pi)} & 0.4e^{i(0\pi)} \\ 0.6e^{i(-0.3\pi)} & 0.2e^{i(-0.3\pi)} & 0.2e^{i(-0.3\pi)} & 0.5e^{i(0.7\pi)} & 0.5e^{i(0.7\pi)} \\ 0 & 0.5e^{i(-0.3\pi)} & 0.5e^{i(0.7\pi)} & 0.3e^{i(-0.3\pi)} & 0.3e^{i(0.7\pi)} \\ 0.25e^{i(-0.2\pi)} & 0.2e^{i(0.8\pi)} & 0.2e^{i(0.8\pi)} & 0.1e^{i(-0.2\pi)} & 0.1e^{i(-0.2\pi)} \\ 0 & 0.3e^{i(-0.2\pi)} & 0.3e^{i(0.8\pi)} & 0.5e^{i(0.8\pi)} & 0.5e^{i(-0.2\pi)} \end{bmatrix}$$

The specific modes (LP_{01} , LP_{11e} , LP_{11o} , LP_{21e} and LP_{21o} modes) can be selectively generated by adjusting specific amplitudes and phases of the input ports. For example, when input ports are setting the same amplitudes and phases, $v^T = [0.4e^{i(0\pi)}, 0.4e^{i(0\pi)}, 0.4e^{i(0\pi)}, 0.4e^{i(0\pi)}, 0.4e^{i(0\pi)}]$. The highly pure LP_{01} mode is obtained in the output port. When the input port information with specific amplitude and phase is applied respectively, $v^T = [0.6e^{i(-0.3\pi)}, 0.2e^{i(-0.3\pi)}, 0.2e^{i(-0.3\pi)}, 0.5e^{i(0.7\pi)}, 0.5e^{i(0.7\pi)}]$. Those beams with the same phase will undergo a specific coupling process to enhance the LP_{11} mode^[26,27].

The evolution process of the beam in the PL is numerically simulated based on the beam propagation method (BPM) algorithm. Figure 2 shows that different input port energy coupling occurs along the direction of propagation in different cross-sections (A–E). After entering the waist region, the light evolves into a corresponding supermode, and then

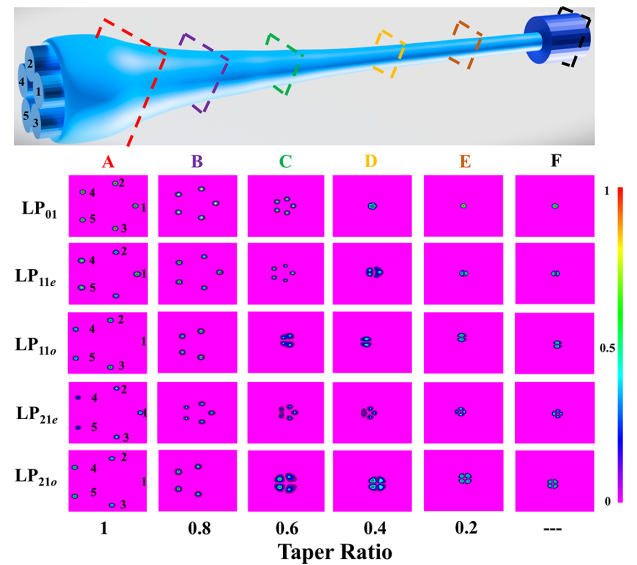


Figure 2. The mode evolution of the 5×1 photonic lantern varies with the taper ratio.

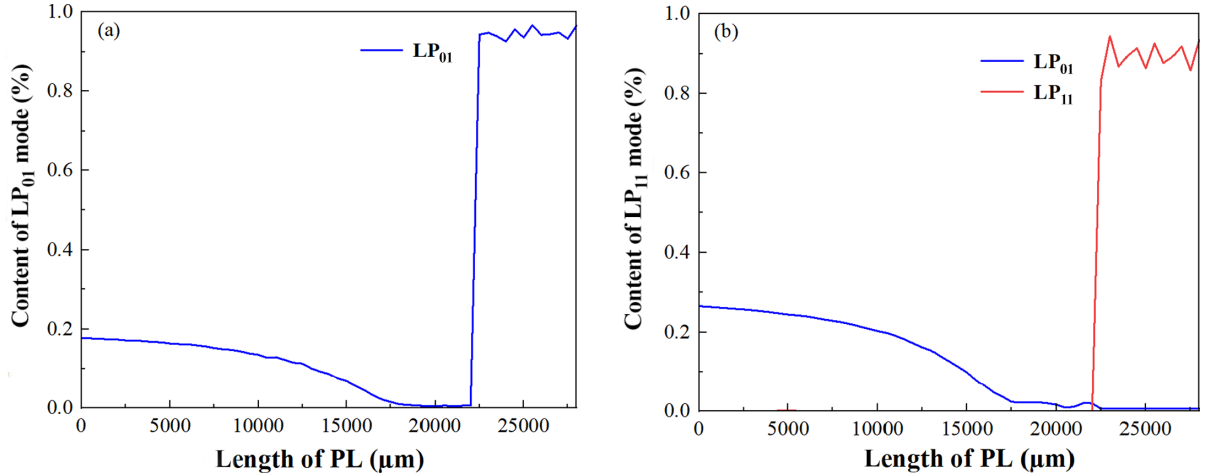


Figure 3. The modal content evolution process in the 5×1 photonic lantern varies with the length of the taper region. (a) Targeting the LP_{01} mode output. (b) Targeting the LP_{11} mode output.

it is transferred into the output port. As an example, we monitor the content of the LP_{01} and LP_{11} modes through the 5×1 PL structure. Figure 3(a) shows that the content of the LP_{01} mode of SMFs gradually decreases along the long taper region, and is steadily maintained at 92% in the MMF. When the LP_{11} mode is regarded as the control target, as shown in Figure 3(b), the content change of the LP_{01} mode presents a similar situation in the taper region. Finally, the content of the LP_{11} mode is stable at about 88%.

3. Experimental setup

The experimental setup of the mode-adaptive control system is shown in Figure 4. The seed is a single-frequency laser operating at a wavelength of 1064 nm. The white noise source (WNS), driven by the radio frequency high-voltage amplifier, applies electrical signals to a LiNbO₃ electro-optic modulator (EOM), thereby achieving spectrum broadening to enhance the SBS threshold. The splitter can divide light into five equal parts. The phases of input SMFs are controlled

by the phase modulators (PMs). The delay lines (DLs) are used to match the optical path difference (OPD) of each input port. The isolators (ISOs) are fusion spliced with band-pass filters (BPFs), and this setup simultaneously filters out background spectral noise and isolates the reverse power.

The amplification system adopts two-stage amplification technology. In the preamplifier systems, the output beam of the PL serves as the seed for the amplifier. The 976 nm laser diodes (LDs) are combined to pump 30/250 μm gain fiber (NA ~ 0.066) via a $(6 + 1) \times 1$ pump and signal combiner, and achieve a total output power of 40 W. The 915 and 981 nm semiconductor lasers are used to precisely control the pump absorption coefficient. The absorption coefficient of the gain fiber for pump light can be adjusted by combining 915 and 981 nm pumping, which allows the thermal load per meter of the gain fiber to be controlled within a suitable range. Therefore, the fiber length is also controlled within a suitable range, which allows for simultaneous suppression of the transverse mode instability (TMI) and SBS effects at kW-level output power^[28]. The main amplifier consists of a 42/250 μm Yb-doped fiber

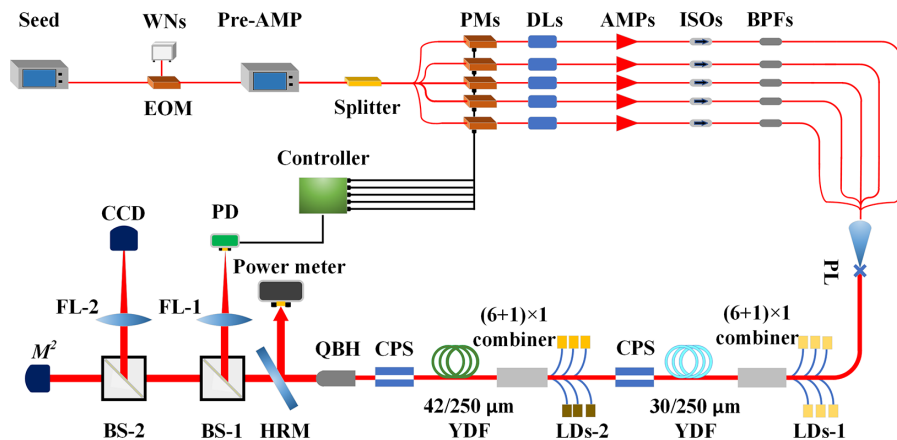


Figure 4. The mode-adaptive control system based on a 5×1 photonic lantern.

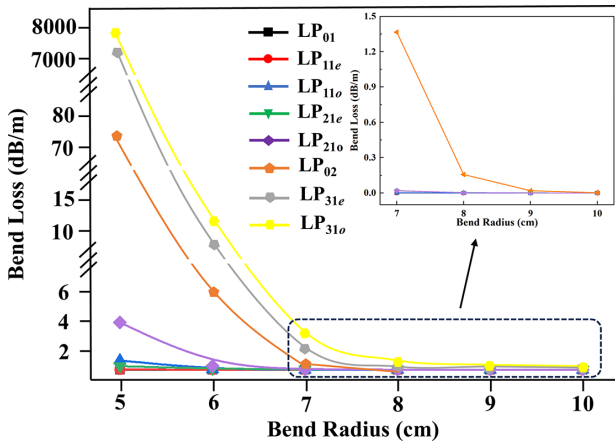


Figure 5. Bend loss of different modes versus bend radius.

(NA ~ 0.069) and a $(6 + 1) \times 1$ signal-pump combiner. Finally, a quartz block holder (QBH) embedded with cladding power strippers (CPSs) is fused for simultaneously filtering excess pump light and outputting the beam.

The beam is received by an M^2 analyzer and a charge-coupled device (CCD) for the purpose of beam quality evaluation. The power-in-the-bucket (PIB) detected by a photonic detector (PD) is used as the evaluation function of the stochastic parallel gradient descent (SPGD) algorithm. By measuring the corresponding change in intensity at the source, an approximate gradient with respect to the phase of each element can be calculated. The controller has an execution speed of more than 500,000 times per second. Thus, the phase-locked loop convergence can be completed within less than 100 iterations^[29].

When the laser system operates at high power, the LMA active fiber inevitably excited excessively more HOMs. For gain fiber with a core diameter of 42 μm , over 20 modes can be supported. We employed the method of bending the fiber to reduce the number of modes in the LMA fibers^[30].

The FM and HOM losses with respect to the bending radius are illustrated in Figure 5. As the bending radius decreases, the bend loss of both the FM and HOM increases nonlinearly. Notably, the HOM shows a stronger sensitivity to the physical deformation of fiber bending, and its bending loss demonstrates a more pronounced increasing trend compared to lower-order modes. Controlling the bending radius of LMA fibers serves dual objectives. Firstly, the bend losses of LP_{01} , LP_{11e} , LP_{11o} , LP_{21e} and LP_{21o} modes maintain a low level, thereby enabling highly efficient and high-purity signal transmission. Secondly, other HOM losses are large enough to have more efficient mode control of the PLs. As depicted in Figure 5, when the bending radius is 7 cm, the bending loss for the LP_{21} mode amounts to 0.02 dB/m, while that of the LP_{02} mode reaches 1.36 dB/m. In the experiment, we choose the bending radius of 7 cm, ensuring that only LP_{01} , LP_{11e} , LP_{11o} , LP_{21e} and LP_{21o} modes can be transmitted in the gain fiber. This approach of employing fiber bending to reduce the number of modes not only reduces mode crosstalk but also enables more precise controlling of the target mode.

For the high-power mode-adaptive control system, the requirements of a high SBS threshold and high coherence of the input ports must be met simultaneously. In order to improve the coherence of each input port, it is essential to utilize a seed laser with narrower spectrum width. However, the reduction in the spectrum linewidth leads to decrease of the SBS threshold, which consequently limits the ability to amplify the output power. Figure 6 shows the SBS threshold of the fiber amplifier within mode control adaptive systems measured at various spectral widths. When the output power exceeds the SBS threshold, a pronounced Stokes peak emerges in the spectrum, as shown in Figure 6(a). The SBS threshold conversion with the spectral width is shown in Figure 6(b). As the spectral width increases, the SBS threshold exhibits a nonlinear increase until the SBS threshold exceeds 1 kW with the spectral width of 18 GHz.

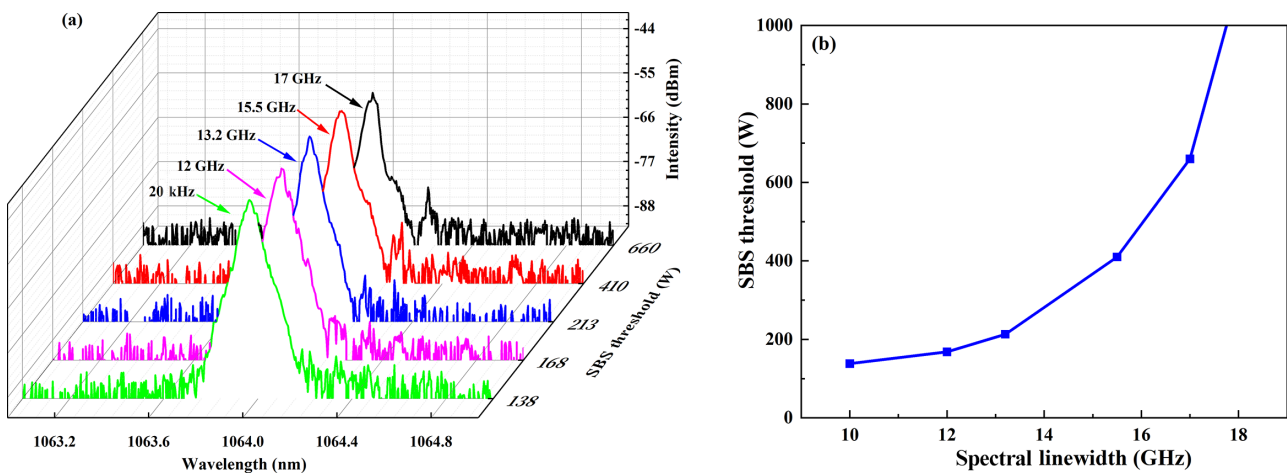


Figure 6. Comparison of the SBS threshold of different 3 dB linewidths. (a) The spectrum of the SBS effect occurring with the different spectral widths. (b) The SBS threshold versus the spectral width.

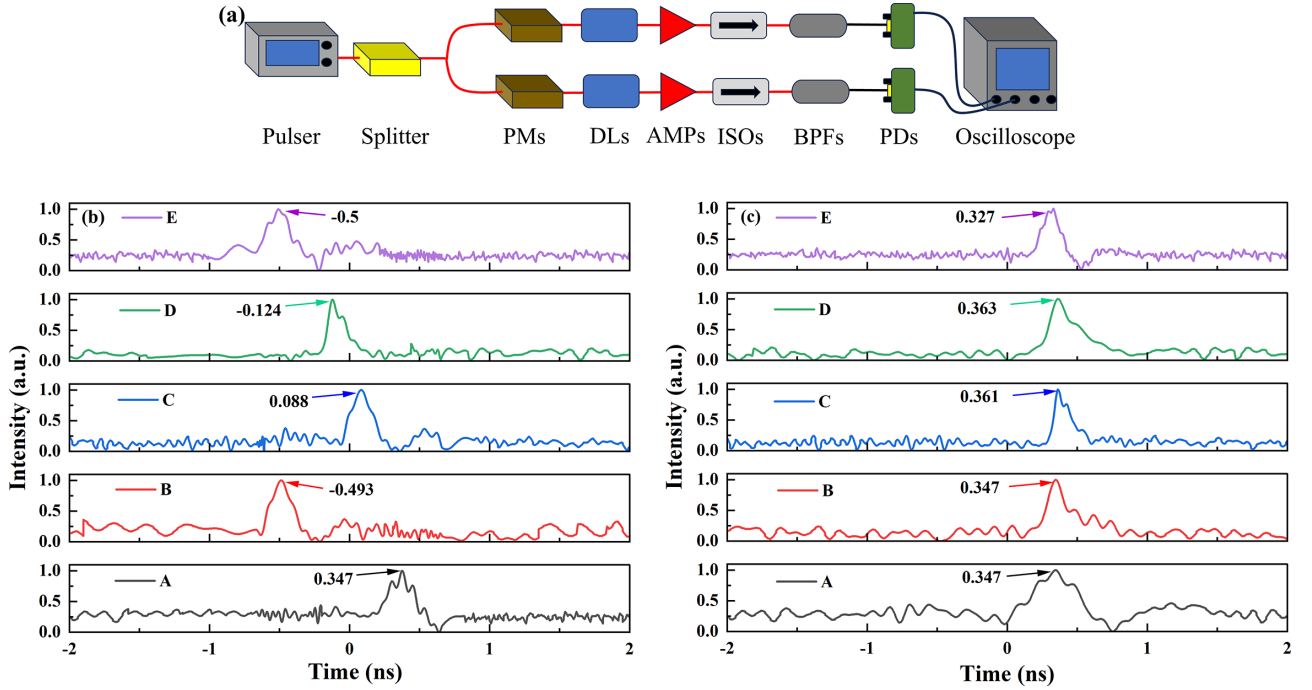


Figure 7. The results of measuring and compensating the OPD. (a) Experimental setup for measuring the OPD of the photonic lantern. OPD among five input ports fiber of the photonic lantern (b) before compensation and (c) after compensation.

However, the corresponding coherence lengths of each input port are only 16 mm with the spectrum width of 18 GHz. To ensure the optical lengths of each input port are precisely confined within the coherence length, it is necessary to employ a high-precision optical metrology technique to measure the fiber length. We utilized a picosecond pulsed laser source (repetition frequency of 9 MHz, pulse width of 1 ns) to measure the OPD of each input port, as shown in Figure 7(a). By analyzing the pulse time delays on the oscilloscope, the differences in the fiber length between the input ports can be measured. Before compensation, Figure 7(b) shows that the minimum OPD is 259 ps, corresponding to the fiber length difference of 5.38 cm. Based on the results, we trimmed the fiber length of each input port, ultimately controlling the OPD within 20 ps, corresponding to the fiber length difference of 4.3 mm, as shown in Figure 7(c). This value falls within the adjustable range of the DLs, ensuring precise phase matching and optimal system performance.

Through the implementation of fiber bending, spectral linewidth optimization and OPD adjustment, we demonstrate a mode-adaptive control system based on a 5×1 PL, which enables effective mode control and power scaling in 42- μm LMA fiber lasers with a minimized number of control ports.

4. Results and discussion

When the FM is designated as the control target mode, the output characteristics of the fiber amplifier based on

the PL are investigated first. The output power conversion with the pump power is shown in Figure 8(a). As the pump power increases, the output power exhibits a linear and stable increase. Finally, more than 1 kW output power is achieved with an optical conversion efficiency of 73%. For conventional fiber lasers, further power amplification may be limited by SBS and TMI. However, in a PL-based fiber laser, the SBS threshold in the amplifier can be well suppressed by tuning the seed linewidth and the optical path of the input ports. Meanwhile, the high-frequency disturbance in the PL will set up a fast refreshed multi-mode interference optical field to disrupt the thermally induced refractive index in the gain fiber. So, the PL-based fiber laser will suppress the TMI well in LMA fiber. In Figure 8(b), a pure output spectrum without nonlinear characteristic peaks is presented with different output powers. Meanwhile, the detailed spectra of the signal laser at different pump powers are also measured and are shown in Figure 8(c).

The SPGD algorithm adaptively controls the phase of the input port fiber by utilizing the maximum PIB as the evaluation function. At the maximum output power, the on-axis signal of the PD changing over time is as shown in Figure 9(a). Before the control is turned on, the output field is generally a superposition of the FM and the HOMs, and the voltage signal exhibits significant fluctuations. After the control is turned on, a stable high-level signal is received by the PD. Figure 9(b) shows the beam quality and the content of LP_{01} mode of the output laser versus the output power. The M^2 factor of the seed laser is 1.28; after passing

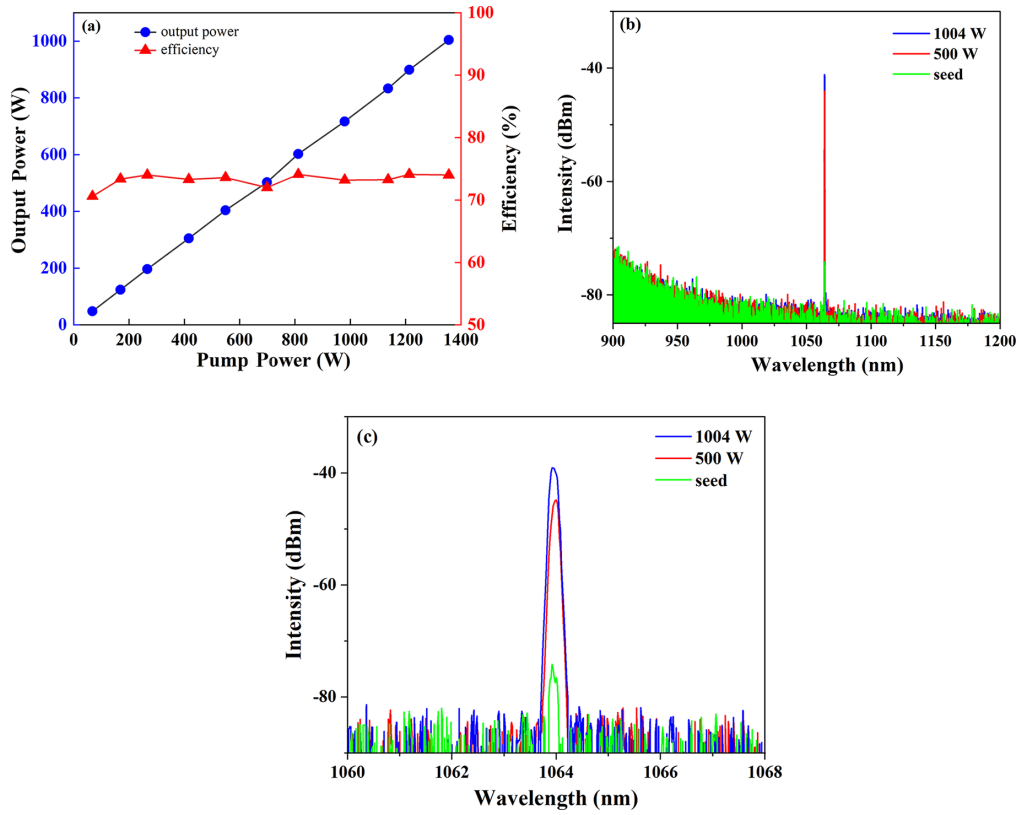


Figure 8. Output properties of the fiber amplifier based on the 5×1 photonic lantern. (a) Output power and efficiency versus pump power. (b) Spectra at different output powers. (c) Detailed spectra at different output powers.

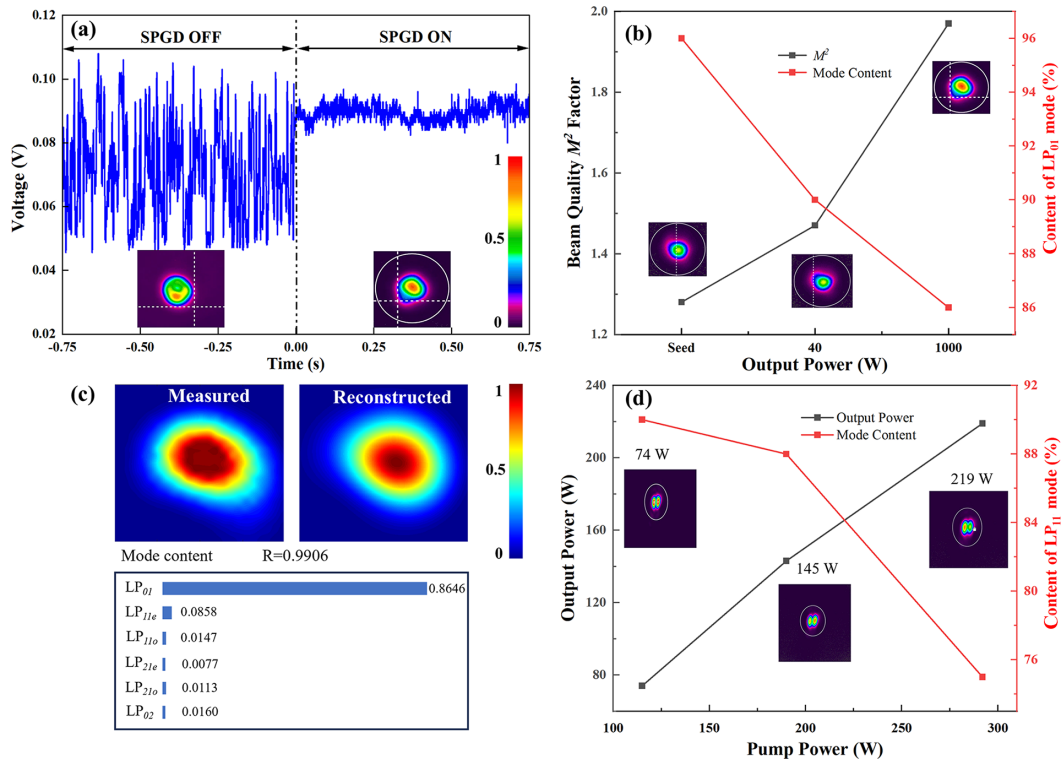


Figure 9. Beam profiles of the 5×1 photonic lantern amplifier. (a) PD signal over time when the SPGD was turned off and on. (b) Beam quality and mode content versus the LP_{01} output power. (c) Mode decomposition of the obtained beam. (d) Output power and mode content of the LP_{11} mode versus the pump power (insets: beam profiles).

Table 1. Output performances of mode-selective operation in a fiber laser with different methods.

Method	Gain fiber (μm)	Output power of LP ₀₁ mode	Output power of LP ₁₁ mode	Ref.
Long-period grating	25/250	117 W	117 W	[3]
Long-period grating	25/250	56.79 W	54.51 W	[32]
Fiber squeezer	20/400	500 W	500 W	[33]
Fiber squeezer	25/400	1389 W	1396 W	[34]
Photonic lantern	13/163	90 mW	80 mW	[35]
Photonic lantern	25/250	4.9 W	4.9 W	[36]
Photonic lantern	42/250	1007 W	219 W	This work

through the pre-amplification it is reduced to 1.47. Then at the highest output power of 1007 W, the M^2 factor is 1.97. As the pump power increases, the modal content of the LP₀₁ mode attenuates from 96% to 86%. The complete mode decomposition effect is evaluated by the numerical method^[31]. The mode decomposition results are shown in Figure 9(c). The modal content of the LP₀₁ mode is 86.46% with the output power of 1 kW. The correlation coefficient between the measured spot and the reconstructed spot is 0.9906. Furthermore, the system demonstrates the capability to generate HOMs. When the target mode is set to the LP₁₁ mode, the output characteristics of the fiber amplifier are as shown in Figure 9(d). The LP₁₁ mode output was achieved at the output power of 219 W with a high optical conversion efficiency of 75%. However, this system creates more intense mode competition after the amplifier, and then the LP₁₁ modal content caused a drop from 90% to 75%.

There has always been an extreme challenge in achieving high-power HOM output in LMA fiber lasers. As shown in Table 1, the previous work of other groups has been focused on mode-selective operation in the fiber laser with core diameters below 25 μm . The previous work of our group only achieved near-FM output at the kilowatt level, but was not capable of controlling high-order modes^[24]. Lu *et al.*^[26] only achieved a 50-W HOM output. In this paper, for the first time, we have simultaneously realized a kilowatt-level FM and a hundred-watt-level HOM in a 42- μm LMA fiber laser.

We observe that, despite the PL exhibiting good mode control ability for the LMA fiber amplifier, the beam quality of the LP₀₁ mode and the purity of the LP₁₁ mode appeared to undergo a certain degradation phenomenon with the increase of pump power. The decrease of beam quality and mode purity is primarily attributed to the transverse spatial-hole burning effect and the spatial mode competition in the LMA fiber amplifiers. In the next step, the implementation of specialty fibers, such as tapered fibers, could be strategically employed to mitigate the transverse spatial-hole burning effect and consequently enhance the mode purity^[37,38].

5. Conclusion

In this work, we demonstrate mode-adaptive control of a kilowatt-level LMA fiber laser, in which a 5×1 PL is

used as a mode converter to generate the FM and HOMs. Consequently, for the LP₀₁ mode control, a total of 1007 W output power with 18 GHz linewidth is obtained with a slope efficiency of 73%. We also achieve a stable LP₁₁ mode output with an output power of 219 W and a high optical conversion efficiency of 75%. The application of the few-port PL in mode-adaptive control of an LMA fiber laser exhibits significant potential for high-power operation of a specific mode in fiber lasers.

Acknowledgement

This work was supported by the National Natural Science Foundation of China (Grant No. 12074432).

References

1. A. Bouhelier, F. Ignatovich, A. Bruyant, C. Huang, G. C. des Francs, J. C. Weeber, A. Dereux, G. P. Wiederrecht, and L. Novotny, *Opt. Lett.* **32**, 2535 (2007).
2. P. Lebegue, J. De Sousa, C. Rapenau, D. Badarau, J. Andrieu, P. Audebert, F. Druon, and D. Papadopoulos, *High Power Laser Sci. Eng.* **13**, e4 (2025).
3. T. Liu, S. Chen, X. Qi, and J. Hou, *Opt. Express* **24**, 27821 (2016).
4. P. Ma, T. Yao, W. Liu, Z. Pan, Y. Chen, H. Yang, Z. Chen, Z. Wang, P. Zhou, and J. Chen, *High Power Laser Sci. Eng.* **12**, e67 (2024).
5. J. Ye, J. Xu, J. Song, Y. Zhang, H. Zhang, H. Xiao, J. Leng, and P. Zhou, *Photonics Res.* **7**, 977 (2019).
6. Y. Zheng, Y. Yang, J. Wang, M. Hu, G. Liu, X. Zhao, X. Chen, K. Liu, C. Zhao, B. He, and J. Zhou, *Opt. Express* **24**, 2063 (2016).
7. A. Kobayakov, M. Sauer, and D. Chowdhury, *Adv. Opt. Photonics* **2**, 1 (2010).
8. S. Ren, W. Lai, G. Wang, W. Li, J. Song, Y. Chen, P. Ma, W. Liu, and P. Zhou, *Opt. Express* **30**, 7845 (2022).
9. M. A. Shevchenko, V. I. Grebenkin, M. V. Tareeva, A. D. Kudryavtseva, L. L. Chaikov, and N. V. Tcherniega, *Bull. Lebedev Phys. Inst.* **45**, 397 (2018).
10. L. Dong, *J. Lightwave Technol.* **40**, 4795 (2022).
11. C. Jauregui, C. Stihler, and J. Limpert, *Adv. Opt. Photonics* **12**, 429 (2020).
12. H. Li, J. Zang, S. Raghuraman, S. Chen, C. Goel, N. Xia, A. Ishaaya, and S. Yoo, *Opt. Express* **29**, 21992 (2021).
13. J. Song, S. Ren, G. Wang, H. Yang, Y. Chen, P. Ma, W. Liu, L. Huang, Z. Pan, and P. Zhou, *J. Lightwave Technol.* **40**, 5668 (2022).
14. M. Chen, J. Cao, Q. Zhang, A. Liu, S. Zhou, Z. Huang, Z. Wang, and J. Chen, *Opt. Express* **32**, 13111 (2024).

15. B. Pulford, R. Holten, T. Matniyaz, M. T. Kalichevsky-Dong, T. W. Hawkins, and L. Dong, *Proc. SPIE* **11981**, 1198100 (2022).
16. Z. Xing, X. Wang, S. Lou, W. Zhang, S. Yan, and Z. Tang, *J. Opt.* **21**, 096731 (2019).
17. F. Anelli, A. Annunziato, A. M. Loconsole, S. Venck, S. Cozic, and F. Prudenzeno, *J. Lightwave Technol.* **43**, 280 (2025).
18. D. Choudhury, D. K. McNicholl, A. Repetti, I. Gris-Sanchez, S. Li, D. B. Phillips, G. Whyte, T. A. Birks, Y. Wiaux, and R. Thomson, *Nat. Commun.* **11**, 5217 (2020).
19. Y. Ding, J. Li, S. Li, Y. Qin, Z. Zhang, X. Wang, Y. Guo, X. Meng, and H. Du, *J. Lightwave Technol.* **41**, 739 (2023).
20. S. G. Leon-Saval, A. Argyros, and J. Bland-Hawthorn, *Nanophotonics* **2**, 429 (2013).
21. S. G. Leon-Saval and IEEE, in *23rd Opto-Electronics and Communications Conference (OECC)* (2018).
22. J. Montoya, C. Hwang, D. Martz, C. Aleshire, T. Y. Fan, and D. J. Ripin, *Opt. Express* **25**, 27543 (2017).
23. J. Montoya, C. Aleshire, C. Hwang, N. K. Fontaine, A. Velazquez-Benitez, D. H. Martz, T. Y. Fan, and D. Ripin, *Opt. Express* **24**, 3405 (2016).
24. Y. Ze, P. Liu, H. Zhang, Y. Hu, L. Ding, B. Yan, J. Zhang, Q. Zhou, and W. Liu, *Opt. Express* **32**, 35794 (2024).
25. Y. Lu, Z. Chen, W. Liu, M. Jiang, J. Yang, Q. Zhou, J. Zhang, J. Chai, and Z. Jiang, *Opt. Express* **30**, 22435 (2022).
26. Y. Lu, Z. Jiang, Z. Chen, M. Jiang, J. Yang, Q. Zhou, J. Zhang, D. Zhang, J. Chai, H. Yang, and W. Liu, *J. Lightwave Technol.* **41**, 5607 (2023).
27. Y. Lu, Z. Jiang, H. Xiao, Z. Chen, M. Jiang, J. Chai, H. Yang, L. Ding, D. Zhang, J. Zhang, Q. Zhou, and W. Liu, *Front. Phys.* **11**, 1198092 (2023).
28. Y. Wen, P. Wang, B. Yang, H. Zhang, X. Xi, X. Wang, and X. Xu, *Photonics* **9**, 716 (2022).
29. Y. Ze, P. Liu, H. Zhang, Y. Hu, L. Ding, B. Yan, J. Zhang, Q. Zhou, and W. Liu, *Micromachines* **15**, 1342 (2024).
30. H. Wang, M.-Y. Chen, Y.-F. Zhu, S.-Y. Li, P. Yin, X.-S. Wu, R.-H. Li, Z.-M. Cai, P.-P. Fu, H. Qin, and J. Wei, *Opt. Eng.* **56**, 016103 (2017).
31. O. Shapira, A. F. Abouraddy, J. D. Joannopoulos, and Y. Fink, in *Conference on Lasers and Electro-Optics (CLEO)* (2015), paper CThB2.
32. X. Yang, Z.-H. Xu, S.-P. Chen, and Z.-F. Jiang, *Opt. Express* **26**, 13740 (2018).
33. R. Su, B. Yang, X. Xi, P. Zhou, X. Wang, Y. Ma, X. Xu, and J. Chen, *Opt. Express* **25**, 23275 (2017).
34. Y. You, G. Bai, X. Zou, X. Li, M. Su, H. Wang, Z. Quan, M. Liu, J. Zhang, Q. Li, H. Shen, Y. Qi, B. He, and J. Zhou, *J. Lightwave Technol.* **39**, 2536 (2021).
35. N. Wang, J. C. A. Zacarias, J. E. Antonio-Lopez, Z. S. Eznavah, C. Gonnet, P. Sillard, S. Leon-Saval, A. Schulzgen, G. Li, and R. Amezcua-Correa, *Opt. Express* **26**, 32777 (2018).
36. S. Wittek, R. B. Ramirez, J. A. Zacarias, Z. S. Eznavah, J. Bradford, G. L. Galmiche, D. Zhang, W. Zhu, J. Antonio-Lopez, L. Shah, and R. A. Correa, *Opt. Lett.* **41**, 2157 (2016).
37. A. P. Napartovich and D. V. Vysotsky, *Phys. Rev. A* **76**, 063801 (2007).
38. Z. Jiang and J. R. Marcianite, *J. Opt. Soc. Am. B* **25**, 247 (2008).